

Stochastic Electron Acceleration in the TeV Supernova Remnant RX J1713.7-3946: The High-Energy Cut-off

Zhonghui Fan^{1*}, Siming Liu^{2†} and Christopher L. Fryer^{3,4‡}

¹*Department of Physics, Yunnan University, Kunming 650091, Yunnan, China*

²*Department of Physics and Astronomy, University of Glasgow, Glasgow, G12 8QQ, UK*

³*Los Alamos National Laboratories, Los Alamos, NM 87545*

⁴*Physics Department, University of Arizona, Tucson AZ 85721*

ABSTRACT

In the leptonic scenario for TeV emission from a few well-observed shell-type TeV supernova remnants (STTSNRs), very weak magnetic fields are inferred. If fast-mode waves are produced efficiently in the shock downstream, we show that they are viable agents for acceleration of relativistic electrons inferred from the observed spectra even in the subsonic phase, in spite that these waves are subject to strong damping by thermal background ions at small dissipation scales. Strong collisionless non-relativistic astrophysical shocks are studied with the assumption of a constant Alfvén speed in the downstream. The turbulence evolution is modeled with both the Kolmogorov and Kraichnan phenomenology. Processes determining the high-energy cutoff of nonthermal electron distributions are examined. The Kraichnan models lead to a shallower high-energy cutoff of the electron distribution and require a lower downstream density than the Kolmogorov models to fit a given emission spectrum. With reasonable parameters, the model explains observations of STTSNRs, including recent data obtained with the *Fermi* γ -ray telescope. More detailed studies of the turbulence generation and dissipation processes, supernova explosions and progenitors are warranted for better understanding the nature of supernova shocks.

Key words: acceleration of particles – MHD – plasmas – shock waves – turbulence – ISM: supernova remnants.

1 INTRODUCTION

The acceleration of cosmic rays up to $\sim 10^{15}$ eV has been attributed to supernova explosions and TeV emission is expected from the remnants (Ginzburg & Ptuskin 1976; Lagage & Cesarsky 1983; Reynolds 2008; Butt et al. 2009). The standard diffusive shock particle acceleration (DSA) model has been successful in explaining emissions from most supernova remnants (Eichler 1979c; Blandford & Eichler 1987; Kirk & Duffy 1999; Zirakashvili & Aharonian 2007; Vannoni et al. 2009; Reynolds 2008). Investigations of acceleration by a spectrum of turbulent plasma waves, the so-called stochastic particle acceleration (SA), also have a long and resilient history (Scott & Chevalier 1975; Lacombe 1977; Achterberg 1979; Eilek 1979; Bykov & Toptygin 1983; Cowsik & Sarkar 1984; Ptuskin 1988; Bykov & Toptygin 1993; Atoyan et al. 2000; Petrosian & Liu 2004; Cho & Lazarian 2006; Liu et al. 2008a). Most authors prefer the use of relativistic leptons to account for the nonthermal radio, X-rays, and TeV emissions from the remnants. The TeV emission has also been attributed to energetic protons and ions (Aharonian et al. 2006; Morlino et al. 2009; Fang et al. 2009; Zirakashvili & Aharonian 2010).

Although the DSA can naturally give a universal power-law energetic particle distribution with the spectral index determined by the shock compression ratio for a linear model, it requires well-defined shock structure and efficient scatter of high-energy particles by small-scale turbulence (Bell 1978). The initial acceleration of low-energy particles to a high enough energy for the shock to be effective, the so-called injection problem, is likely due to the SA by turbulence. Lacombe (1977)

* E-mail: fanzh@ynu.edu.cn

† E-mail: sliu@astro.gla.ac.uk

‡ E-mail: fryer@lanl.gov

showed that the SA by small-scale Alfvén waves can be more efficient than the first order Fermi acceleration by shocks. Achterberg (1979) derived approximate diffusion coefficients and showed that stochastic interactions of particles with a spectrum of plasma waves can lead to efficient particle acceleration. Over the past few decades, the SA has also been explored for broader astrophysical applications (e.g., Eichler 1979a,b; Cowsik & Sarkar 1984; Ball, Melrose, & Norman 1992; Miller, LaRosa & Moore 1996; Schlickeiser & Miller 1998; Petrosian & Liu 2004; Yan & Lazarian 2004; Fisk & Gloeckler 2007; Petrosian & Bykov 2008). The essential challenges to the SA model are a self-consistent treatment of the nonlinear turbulence spectral evolution and the requirement of the same energy dependence of the acceleration and escape timescales for the production of a power-law particle distribution (Ball, Melrose, & Norman 1992; Becker, Le & Dermer 2006; Ptuskin 1988). Recently Gibbsian theory has been generalized to account for power-law distributions in marginally stable Gibbsian equilibria (Treumann & Jaroschek 2008). It remains to be shown how the physical processes of the SA are related to the ordering parameter κ of this statistics. Most previous studies assume isotropic magnetohydrodynamic (MHD) waves for the turbulence (Lacombe 1977; Achterberg 1979; Eichler 1979b; Miller, LaRosa & Moore 1996). The anisotropy of the turbulence caused by cascade and damping processes has been considered recently (Goldreich & Sridhar 1995; Chandran 2003; Yan & Lazarian 2004; Cho & Lazarian 2006; Jiang et al. 2009). In particular, Liu et al. (2008a) show that the scatter and acceleration rates of charged relativistic particles by fast-mode waves in a high- β plasma may be much higher than those given by the standard quasi-linear theory with an isotropic wave power spectrum.

Over the past few years, detailed radio, X-ray, γ -ray, and TeV observations of a few shell-type TeV supernova remnants (STTSNRs) pose several challenges to the classical DSA model in the hadronic scenario, where the TeV emission is produced through neutral pion decays induced by proton-proton scatter (Aharonian et al. 2006, 2007; Tanaka et al. 2008; Funk 2009). Besides requiring efficient amplification of the magnetic field in the upstream plasma and a good correlation between the magnetic field and background plasma density (Plaga 2008; Fang et al. 2009; Morlino et al. 2009), the model also implies a cosmic ray energy of $\sim 10^{51}$ ergs for each remnant and an electron acceleration efficiency more than 4 orders of magnitude lower than the ion acceleration efficiency (Butt et al. 2008). The high density of the upstream plasma in the model also implies significant thermal X-ray emission from the downstream, which may exceed the observed upper limit (Cassam-Chenaï et al. 2004). A very hard proton spectrum is also required to fit the γ -ray spectrum obtained recently with the *Fermi* γ -ray telescope (Funk 2009). Although these kinds of remnants may be atypical, detailed modeling can still have profound implications for our understanding of supernova shocks (Butt et al. 2009; Zirakashvili & Aharonian 2010).

In a previous paper, we showed that the SA of electrons by turbulent plasma waves in the shock downstream might naturally explain these observations (Liu et al. 2008a). Turbulence is expected given that the size of these remnants are many orders of magnitude larger than the dissipation scale of the ion inertial length (Dickel et al. 1991; Jiang et al. 2009). The DSA model proposes that particle acceleration occurs directly and predominantly at the ion inertial length or gyro-radius (Reynolds 2008). This requires the absence of instabilities over a large range of spatial scales, which is highly idealized. Giacalone & Jokipii (2007) showed that density fluctuations in the upstream can be amplified significantly by shock waves, resulting in strong turbulence in the downstream. Magnetized turbulence appears to be a more generic and natural energy dissipation channel than the short-length-scale shock fronts (SF).

With the leptonic model, the TeV emission is mostly produced by the inverse Comptonization of the cosmic microwave background radiation by TeV electrons (Porter et al. 2006). The magnetic field required to reproduce the observed X-ray flux by the same TeV electrons through the synchrotron process implies a spectral cutoff in the hard X-ray band, which is in agreement with observations. The SA model also requires a much lower gas density than the DSA model, which not only explains the lack of thermal X-ray emission from the shell of the remnants, but also reduces the energetics of the supernovae. The required turbulence generation scale is comparable to the size of the observed X-ray filaments as well (Dickel et al. 1991; Uchiyama et al. 2007). The fast variability of small X-ray features may be attributed to rapid spatial diffusion of high energy electrons (Liu et al. 2008a). As we will show in this paper, the agreement between preliminary results from *Fermi* observations and the model prediction is also impressive (Funk 2009).

The SA by fast-mode waves has been studied by several authors (Bykov & Toptygin 1983; Ptuskin 1988; Bykov & Toptygin 1993; Miller, LaRosa & Moore 1996; Schlickeiser & Miller 1998; Yan & Lazarian 2004; Cho & Lazarian 2006; Liu et al. 2006). Both resonant and nonresonant interactions have been considered. In this paper, we consider the nonresonant acceleration by compressional waves first studied by Bykov & Toptygin (1983); Ptuskin (1988). Compared with these original studies, our model has several distinct features: 1) most of the dissipated fast-mode turbulence energy is absorbed by thermal background ions; 2) the residual fast-mode waves in the dissipation scales propagate along local magnetic fields and preferentially accelerate electrons in the background plasma; 3) the plasma physics processes in the dissipation range in principle lead to a self-consistent treatment of the electron injection process at low energies; 4) the scatter mean-free-path of relativistic electrons, which is a free parameter in most of the previous studies, is determined by the characteristic length of the magnetic field, which in a high- β plasma is reduced by strong turbulence motions significantly; 5) the high-energy cutoff of the particle distribution is tied to the characteristic length of the magnetic field.

In this paper, we first discuss the SA by decaying turbulence in general and show that fast-mode waves may account for observations of a few STTSNRs (Section 2). In Section 3, we present the structure of the downstream turbulence with both

the Kolmogorov and Kraichnan phenomenology for the turbulence cascade. The transit-time damping (TTD) by the thermal background particles of compressional fast-mode turbulence is considered in the dissipation range. The stochastic acceleration of relativistic electrons by fast-mode wave turbulence in the subsonic phase is discussed in Section 4, where physical processes determine the acceleration of the highest energy electrons are discussed. The models are applied to the well-observed TeV SNR RX J1713.7-3946 in Section 5. Although the inferred plasma density is much lower than that in the hadronic scenario, some models still have significantly higher densities than that derived from *XMM-Newton* observations (Cassam-Chenaï et al. 2004). In Section 6, we discuss how the density may be further reduced by considering the turbulence generation processes and first-order Fermi acceleration in the supersonic phase. Conclusions are drawn in Section 7.

2 GENERAL CONSTRAINTS ON THE PARTICLE ACCELERATION

According to the classical Fermi mechanism (Fermi 1949), the particle acceleration rate is determined primarily by the scatter mean-free-path l and the velocity of the scatter agents u (Blandford & Eichler 1987; Ball, Melrose, & Norman 1992). Very general constraints can be obtained on the nature of these processes when applying this mechanism to specific observations. For example, Eichler (1979a) showed that the acceleration process must be selective in the sense that only a fraction of the background particles are accelerated to very high-energies. Otherwise, these stochastic interactions likely lead to plasma heating instead of a very broad energy distribution of accelerated particles as frequently observed in dynamically evolving collisionless astrophysical plasmas. For particle acceleration in solar flares, Eichler (1979b) argued that this selective acceleration could be achieved in the energy domain (i.e., the frequency domain for the waves) through cyclotron resonances of particles with a spectrum of cascading plasma waves. In the DSA model, the particle acceleration at low energies and the shock structure determine the efficiency of different particle species (Eichler 1979a). In the presence of a magnetic field, selective energization may also be realized in the domain of the particle pitch-angle and/or wave direction angle with respect to the magnetic field (Beresnyak & Lazarian 2008).

Further constraints can be put on the SA by a spectrum of turbulence. Given the small gyro-radii of charged particles in magnetized astrophysical plasmas, charged particles couple strongly through the magnetic field. As a result, the turbulence responsible for the SA will decay as the energy carrying plasma being carried away from the source region of the turbulence by large scale flows and/or magnetic fields for a high and/or low β plasma, respectively. This is the case for the SA in a shock downstream with a high value of the plasma β , where the turbulence is generated at the SF and its intensity decreases as the flow moves away from the SF (Liu et al. 2008a). We next discuss constraints on such a particle acceleration scenario.

In the *Kolmogorov* phenomenology for the turbulence cascade (Kolmogorov 1941), the free energy dissipation rate is given by

$$Q \equiv C_1 \rho u^3 / L, \quad (1)$$

where C_1 is a dimensionless constant, ρ is the mass density, and u and L are the eddy speed and the turbulence generation scale, respectively. The eddy turnover speed and time at smaller scales are given respectively by

$$v_{edd}^2(k) \equiv 4\pi W(k) k^3 \propto k^{-2/3}, \quad (2)$$

$$\tau_{edd}(k) \equiv (k v_{edd})^{-1} = (4\pi W k^5)^{-1/2} \propto k^{-2/3}, \quad (3)$$

where

$$W(k) = (u^2/4\pi)L^{-2/3}k^{-11/3} = (4\pi)^{-1}(Q/C_1\rho)^{2/3}k^{-11/3} \propto k^{-11/3} \quad (4)$$

is the isotropic turbulence power spectrum, $k = 1/l$ is the wave number and l is the eddy size. From the three-dimension Kolmogorov constant $C \simeq 1.62$ (Yeung & Zhou 1997), we obtain $C_1 = C^{-3/2} = 0.485$. At the turbulence generation scale $L = 1/k_m$, $v_{edd} = u$, $Q = C_1\rho[(4\pi W)^3 k^{11}]^{1/2} = C_1\rho v_{edd}^2(k)/\tau_{edd}(k)$, and the total turbulence energy is given by $\int W(k)4\pi k^2 dk = (3/2)u^2$. The turbulence decay time is therefore given by $\tau_d \equiv dt/d \ln(u) = 3\tau_{edd}(k_m)/C_1$, where t indicates the time, i.e., eddies decay after making $3/(2\pi C_1) \sim 1$ turn.

We are interested in the acceleration of particles through scattering randomly with heavy scatter centers with the corresponding acceleration time given by (Blandford & Eichler 1987; Ball, Melrose, & Norman 1992)

$$\tau_{ac} = \tau_{sc}[3v^2/v_{edd}^2(k)], \quad (5)$$

where

$$\tau_{sc} = (kv)^{-1} = l/v \quad (6)$$

is the scatter time, v is the particle speed, and we have assumed that the scatter mean free-path is equal to l . For the above isotropic Kolmogorov turbulence spectrum, $\tau_{ac}(k) = 3v/(4\pi W k^4) \propto k^{-1/3}$. To have significant stochastic particle acceleration, the acceleration time $\tau_{ac}(k)$ should be shorter than the turbulence decay time τ_d , which implies $u^2 > C_1 v v_{edd}(k)$. So, in general,

the SA is more efficient at smaller scales. The onset scale of the SA is given by $k_c = (C_1 v/u)^3 k_m$, where $\tau_{ac} = \tau_d$. Therefore, to produce energetic particles with a speed of v by a Kolmogorov spectrum of scatter centers, the turbulence must have a dynamical range greater than

$$D_{Kol} = (C_1 v/u)^3. \quad (7)$$

This acceleration process corresponds to the acceleration by incompressional motions studied by Bykov & Toptygin (1983).

In the *Iroshnikov—Kraichnan* phenomenology (Iroshnikov 1963; Kraichnan 1965; Jiang et al. 2009), the turbulence cascade rate is suppressed by the wave propagation effect by a factor of v_F/v_{edd} , where v_F (independ of k) is the wave group speed:

$$C_1 \rho v_{edd}^3 / (v_F \tau_{edd}) = Q. \quad (8)$$

Then we have

$$Q = C_1 \rho u^4 / (L v_F), \quad (9)$$

$$W(k) = (u^2 / 4\pi) k_m^{1/2} k^{-7/2}, \quad (10)$$

$$v_{edd} = u (k/k_m)^{-1/4}, \quad (11)$$

$$\tau_{edd} = u^{-1} k_m^{-1/4} k^{-3/4}, \quad (12)$$

$$\tau_{ac} = (3v/u^2) (k_m k)^{-1/2}, \quad (13)$$

and the turbulence decay time is given by

$$\tau_d = 3\tau_{edd}(k_m)v_F/(C_1 u), \quad (14)$$

where the wave speed $v_F \gg u$. To have significant acceleration through scatter with the eddies, the dynamical range of the turbulence must be greater than

$$D_{IK} = (C_1 v/v_F)^2, \quad (15)$$

which is much less than $D_{Kol} = (C_1 v/u)^3$.

The resonant interactions of particles with waves may be more effective in accelerating particles in this case than the interactions with eddies. For a wave phase speed v_F independent of k and a wave spectrum of $W(k) = v_F^2 (4\pi k_m^3)^{-1} (k/k_m)^{-\delta}$, where δ is the wave spectral index, the standard quasi-linear theory gives a scatter time of $\tau_{sc} \simeq (L/v)(r_g k_m)^{4-\delta} = [v_F^2/v_{edd}(r_g^{-1})^2] r_g/v$ for particles with a gyro-radius of $r_g = k_0^{-1}$. And the acceleration time is given by $\tau_{ac} \simeq 3\tau_{sc}v^2/v_F^2 \simeq (3v^2/v_{edd}(k_0)^2)/(v k_0)$, which is essentially the same as equations (5) and (6). Although the acceleration rate depends on the phase speed of these waves, the scatter rate is proportional to the intensity of waves in resonance with the particles. So the acceleration is not enhanced by these kinds of resonant interactions. In the presence of magnetic fields, the stochastic acceleration of charged particles can be very efficient (Chandran 2003). Cho & Lazarian (2006) reviewed several mechanisms by MHD waves, which can accelerate particles within the turnover time of large scale eddies for appropriate particle spatial diffusion coefficients. Some of these mechanisms likely result in plasma heating instead of particle acceleration as the particle energization processes are not selective. The corresponding waves are also likely subject to efficient damping by the thermal background particles. There are other mechanisms, which preferentially accelerate energetic particles.

For isotropic acoustic wave turbulence with a wave phase speed v_F , Ptuskin (1988) showed that the stochastic acceleration timescale of energetic particles with a spatial diffusion coefficient $D = \tau_{sc}v^2/3 > v_F/k_d$ is given by (see also Bykov & Toptygin (1983))

$$\tau_{ac} \simeq [3 + \xi(\delta)(Dk_m/v_F)^{3-\delta}]D/u^2, \quad (16)$$

where $3u^2/2$ is the overall wave intensity, k_m indicates the wave generation scale, and below the turbulence dissipation scale $l_d = 1/k_d$ the wave intensity is negligible. $\xi(\delta)$ depends on δ and is on the order of unity (e.g., $\xi(11/3) \simeq 3.0$). The results for fast and slow diffusion have been combined here approximately to give a unified expression (Ptuskin 1988; Cho & Lazarian 2006). For $\delta < 4$, τ_{ac} increases monotonically with D . To have significant acceleration, the minimum acceleration timescale $\tau_{acmin} = \tau_{sc}v^2/u^2$ must be less than $\tau_d = 3Lv_F/(C_1 u^2)$. Then the scatter mean-free-path of the particles $\tau_{sc}v$ must be shorter than

$$L/D_{AI} = 3Lv_F/(C_1 v) = 3L/D_{IK}^{1/2}. \quad (17)$$

It is also possible that the dynamics of the turbulence cascade is not affected by the wave propagation, which only enhances the particle acceleration rate. Then $\tau_d = 3L/(C_1 u)$, the dynamical range required for the SA to be significant is given by

$$D_{AK} \equiv C_1 v/(3u) = D_{Kol}^{1/3}/3. \quad (18)$$

Several STTSNRs have been observed extensively in the radio, X-ray, and TeV bands. X-ray observations with the

Chandra, *XMM-Newton*, and *Suzaku*, and TeV observations with the HESS have made several surprising discoveries that challenge the DSA model in the hadronic scenario (Aharonian et al. 2006, 2007; Liu et al. 2008a; Tanaka et al. 2008). The leptonic scenario, on the other hand, is relative simple except that the electron acceleration mechanism needs to be addressed (Zirakashvili & Aharonian 2007; Liu et al. 2008a; Vannoni et al. 2009). The TEV SNR RX J1713.7-3946 is about $T_{\text{life}} = 1600$ years old (Wang et al. 1997) with a radius of $R \simeq 10$ pc and a distance of $D \simeq 1$ kpc. By fitting its broadband spectrum with an electron distribution of $f \propto \gamma^{-p} \exp -(\gamma/\gamma_c)^{1/2}$ (the dashed lines in Fig. 7), we find that $p = 1.85$, $B = 12.0 \mu\text{G}$, $\gamma_c m_e c^2 = 3.68$ TeV, and the total energy of relativistic electrons with the Lorentz factor $\gamma > 1800$ $E_e = 3.92 \times 10^{47}$ erg.

The X-ray emitting electrons have a gyro-radius of $r_g \simeq 10^{15}$ cm, which should be shorter than the particle scatter mean-free-path. To produce these electrons through the SA, the turbulence must be generated on scales greater than $D_{Kol}r_g$, $D_{IK}r_g$, $D_{AK}r_g$, and $D_{AI}r_g$ for the non-resonant Kolmogorov, Kraichnan, acoustic Kolmogorov, and Kraichnan phenomenology, respectively. For STTSNRs, $u \sim v_F \sim 0.01c$, $D_{Kol}r_g \sim 10$ kpc, which is much greater than the radii of the remnants. The SA by eddies with a Kolmogorov spectrum is therefore insignificant. The standard quasi-linear theory also predicts negligible SA. $D_{IK}r_g \sim 30$ pc, which is also too thick. $D_{AI}r_g \sim D_{AK}r_g \sim 0.03$ pc, which is much greater than the ion inertial length and may result from Kelvin-Helmholtz instabilities or cosmic ray drifting upstream (Bell 1978; Micono et al. 1999; Giacalone & Jokipii 2007; Niemiec et al. 2008). Therefore if relativistic electrons from the STTSNRs are accelerated through the SA, they may be energized by high-speed compressional plasma waves. Previously Eichler (1979a) showed that the non-selective acceleration as given by equations (5) and (13) leads to plasma heating instead of particle acceleration. Here we give a different argument against these acceleration processes. The acceleration timescale in the following is given by equation (16) with D depending on the wave spectrum and particle energy.

The DSA models are usually favored over the SA models for two main reasons: 1) the DSA can naturally produce a power-law particle distribution; 2) the DSA corresponds to a first-order Fermi mechanism and is presumably more efficient than the SA, which corresponds to a second-order Fermi mechanism. While how shocks produce power-law high-energy particle distributions is relatively well understood, the second reason appears to be a misconception. It is true that the ratios of the acceleration and scatter rates are proportional to the first and second power of the speed ratio of the scatter agent and the particle for the DSA and SA, respectively. But in the DSA models, there are two scatter processes: scatter of particles by turbulence, which causes the particle diffusion, and the particle crossing of the SF due to this diffusion. The SF crossing rate is about a factor of v/u lower than the particle scatter rate by the turbulence for a shock speed of $\sim u$ (Lagage & Cesarsky 1983). As a result, the acceleration rates of the DSA and SA models are both proportional to u^2/lv . Therefore the SA is not necessarily less efficient than the DSA. The SA at small scales can also be enhanced by high speed kinetic plasma waves (Pryadko & Petrosian 1997; Petrosian & Liu 2004). Of course, the speed of the scatter agent accessible to a particle may depend on the scatter mean-free-path l in the SA. The stochastic acceleration rate can be very low if u^2 decreases quickly with the decrease of l . For the DSA and SA by large-scale acoustic waves in the shock downstream, the speed of the scatter agent is proportional to the shock speed. One just needs to reduce the scatter mean-free-path l to enhance the acceleration rate. As we will show in Sections 3 and 4, considering the competition of isotropic cascade with anisotropic damping of fast-mode waves through the transit-time-damping process, the waves in the dissipation range propagate along local magnetic field lines with a spectrum index of 2. In a high- β plasma, the damping is mostly caused by ions. The residual parallel propagating waves however preferentially accelerate electrons. Energetic particles are also subject to efficient acceleration by large-scale fast-mode (acoustic) waves with energy independent acceleration and scatter rates, giving rise to power-law particle distributions in the steady-state. At even higher energies, the gyro-radius of the particles exceeds the characteristic length of the magnetic field, which also corresponds to the dissipation scale, the spatial diffusion coefficient D increases quickly with energy. However, due to interactions with large-scale turbulence, both the acceleration and spatial diffusion timescales vary gradually with D , implying a gradual high-energy cutoff.

3 SHOCK STRUCTURE AND DAMPING OF FAST-MODE WAVES IN THE DOWNSTREAM

We consider the relatively simple case, where both the thermal pressure and magnetic field are negligible in the upstream and the shock normal is parallel to the plasma flow. The mass, momentum, and energy fluxes are given, respectively, by ρV_0 , $P + \rho V_0^2$, and $V_0(E + P + \rho V_0^2/2)$, where V_0 , P , and E are the speed, pressure, and energy density of the plasma flow, respectively. Based on the parameters inferred from the leptonic scenario for the TeV emission from STTSNRs shown in Section 2, the plasma β in the shock downstream is likely high and the fast-mode wave damping by thermal background is then dominated by protons and ions (Liu et al. 2008a). The Alfvén speed given by $v_A = (B^2/4\pi\rho)^{1/2}$ therefore must be much smaller than the turbulence speed u near the shock front, where B is the magnetic field intensity. For strong non-relativistic shocks with the shock frame upstream speed U much higher than the speed of the parallel propagating fast mode waves in the upstream $v_F = (v_A^2 + 5v_S^2/3)^{1/2}$, where $v_S^2 = P_g/\rho$ is the isothermal sound speed and P_g is the thermal pressure of the gas, $V_0 = U$ and $\rho U^2 \gg P \sim E$ in the upstream. In the downstream, the pressure and energy density have contributions from the thermal gas and turbulence: $P = \rho(v_S^2 + u^2)$ and $E = \rho(3v_S^2/2 + 3u^2/2)$, where we have assumed that the turbulence behaves

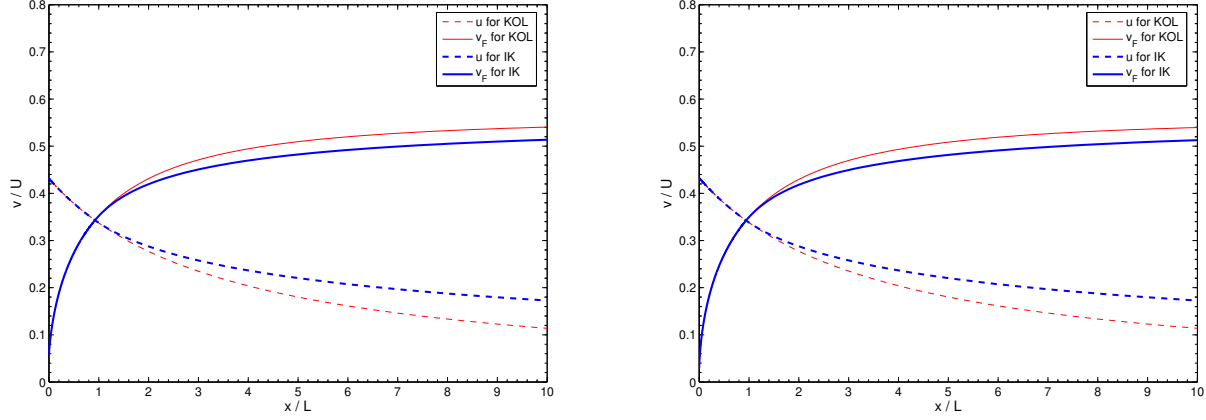


Figure 1. Evolution of the eddy speed u and the speed of parallel propagating fast mode waves v_F in the downstream. The thick and thin lines are for the Kraichnan with $v_A = 0.036U$ (left) and Kolmogorov with $v_A = 0.018U$ (right) phenomenology, respectively.

as an ideal gas and ignored possible dynamical effects of the wave propagation. Then we have (Tidman & Krail 1971)

$$\rho_u U = \rho_d U/4, \quad (19)$$

$$\rho_u U^2 = \rho_d (U^2/16 + v_S^2 + u^2), \quad (20)$$

$$\rho_u U^3/2 = \rho_d U (U^2/16 + 5v_S^2 + 5u^2)/8, \quad (21)$$

where the subscripts u and d denote the upstream and downstream, respectively, and we have ignored the effects of the electromagnetic fields and the thermal energy and pressure in the upstream. Then we have

$$U^2 = 5v_S^2 + 5u^2 + U^2/16. \quad (22)$$

This is slightly different from that given by Liu et al. (2008a), where we assumed that the pressure and enthalpy of the turbulent magnetic field are given by $\rho_d v_A^2/3$ and $5\rho_d v_A^2/6$, respectively.

The shock structure can be complicated due to the present of turbulence. We assume that the turbulence is generated isotropically and has a generation scale of L , which does not change in the downstream. The speeds v_S , v_A , and u therefore should be considered as averaged quantities on the scale L . v_A depends on the upstream conditions and/or the dynamo process of magnetic field amplification (Lucek & Bell 2000; Cho & Vishniac 2000; Niemiec et al. 2008). Here we assume it a constant in the downstream. One can then quantify the evolution of other speeds in the downstream.

For the Kolmogorov phenomenology (Zhou & Matthaeus 1990),

$$\frac{3d\rho u^2}{2dt} = -Q \quad \text{i.e.,} \quad \frac{3Udu(x)^2}{8dx} = -\frac{C_1 u(x)^3}{L}. \quad (23)$$

Near the SF, we denote the isothermal sound speed and Alfvén speed by v_{S0} and v_{A0} , respectively. Then the eddy speed at the SF is given by $a^{1/2}U/4$ with $a = 3 - 16v_{S0}^2/U^2$. Integrate equation (23) from the SF ($x = 0$) to downstream ($x > 0$), we then have

$$\frac{u(x)}{U} = \frac{1}{4C_1 x/3L + 4/a^{1/2}}, \quad (24)$$

$$\frac{v_S(x)}{U} = \left[\frac{3}{16} - \frac{1}{16(C_1 x/3L + a^{-1/2})^2} \right]^{1/2}, \quad (25)$$

$$\frac{v_F(x)}{U} = \left[\frac{5}{16} - \frac{5}{48(C_1 x/3L + a^{-1/2})^2} + \frac{v_A^2}{U^2} \right]^{1/2}. \quad (26)$$

As mentioned in Section 2, to produce the observed X-ray emitting electrons in the STTSNRs through the SA processes, fast-mode waves needs to be excited efficiently. The MHD wave period is given by $\tau_F(k) = 2\pi/v_F k$. Then the transition from the Kolmogorov to Kraichnan phenomenology occurs at the scale, where $\tau_F(k_t) = 2\pi\tau_{\text{edd}}(k_t)$ or $v_F = v_{\text{edd}}(k_t)$ (Jiang et al. 2009). We then have

$$k_t = (u/v_F)^3 k_m. \quad (27)$$

For $k_t > k > k_m$, the turbulence spectrum is Kolmogorov like given by equation (4). For $k > k_t > k_m$, the turbulence spectrum in the inertial range is given by

$$W(k) = \frac{1}{4\pi} \begin{cases} v_F^{1/2} u^{3/2} k_m^{1/2} k^{-7/2} & \text{for IK,} \\ u^2 k_m^{2/3} k^{-11/3} & \text{for Kol.} \end{cases} \quad (28)$$

Although the turbulence energy exceeds $(3/2)u^2$ when the wave propagation effect is considered, we still assume that the enthalpy of the turbulence is given by $(5/2)u^2$ for $v_F < u$ so that equation (22) and the above solutions for the speed profiles remain valid.

In the subsonic phase with $v_F > u$,

$$W(k) = \frac{u^2}{4\pi} \begin{cases} k_m^{1/2} k^{-7/2} & \text{for IK,} \\ k_m^{2/3} k^{-11/3} & \text{for Kol.} \end{cases} \quad (29)$$

and

$$\frac{3Udu(x)^2}{8dx} = -\frac{C_1 u(x)^4}{Lv_F} \quad \text{for IK,} \quad (30)$$

where from equation (22) one has $v_F = [5U^2/16 + v_A^2 - 5u^2(x)/3]^{1/2}$. Equation (30) can be solved numerically to get the speed profiles in the subsonic phase. Figure 1 shows the v_F and u profiles with $v_A = v_{A0} = v_{S0} \ll U$ in the downstream. The thick and thin lines are for the Kraichnan and Kolmogorov phenomenology, respectively.

In summary, for $k > \max(k_m, k_t)$, the turbulence spectrum in the inertial range is given by

$$W(k) = \frac{1}{4\pi} \begin{cases} u^{3/2} \min(v_F^{1/2}, u^{1/2}) k_m^{1/2} k^{-7/2} & \text{for IK,} \\ u^2 k_m^{2/3} k^{-11/3} & \text{for Kol,} \end{cases} \quad (31)$$

and for $k_t > k > k_m$, $W(k) = u^2 (4\pi)^{-1} k_m^{2/3} k^{-11/3}$.

The transit-time damping (TTD) of compressional fast-mode waves starts at the characteristic length of the magnetic field $l_d = 1/k_d$, where the Alfvén speed is comparable to the eddy speed, i.e.,

$$v_A^2 = 4\pi W(k_d) k_d^3 = \begin{cases} \min(v_F^{1/2}, u^{1/2}) u^{3/2} k_m^{1/2} k_d^{-1/2} & \text{for IK,} \\ u^2 (k_m/k_d)^{2/3} & \text{for Kol.} \end{cases} \quad (32)$$

At even larger scales, the vortex motions produce random magnetic fields comparable with the mean field reducing the scatter mean-free-path of charged background particles to l_d or even shorter scales. This trapping of charged particles within a scale of l_d prevents the TTD on scales above l_d . The incompressional modes are not subject to the TTD and have different spectra (Goldreich & Sridhar 1995; Cho & Lazarian 2006). In what follows, we only consider the compressional (fast magnetosonic) wave modes. Then we have

$$k_d = k_m (u^3/v_A^3) \begin{cases} \min(v_F, u)/v_A & \text{for IK,} \\ 1 & \text{for Kol.} \end{cases} \quad (33)$$

Since $v_F > v_A$, one has $k_t < k_d$, and damping is negligible in the regime, where $k_t > k > k_m$.

For a fully ionised hydrogen plasma with isotropic particle distributions, which is reasonable in the absence of strong large-scale magnetic fields, the TTD rate is given by (Stix 1962; Petrosian et al. 2006)

$$\Lambda_T(\theta, k) = \frac{(2\pi k_B)^{1/2} k \sin^2 \theta}{2(m_e + m_p) \cos \theta} \times \left[(T_e m_e)^{1/2} e^{-\frac{m_e \omega^2}{2k_B T_e k_{\parallel}^2}} + (T_p m_p)^{1/2} e^{-\frac{m_p \omega^2}{2k_B T_p k_{\parallel}^2}} \right] \quad (34)$$

where k_B , T_e , T_p , m_e , m_p , θ , ω , and $k_{\parallel} = k \cos \theta$ are the Boltzmann constant, electron and proton temperatures and masses, angle between the wave vector and mean magnetic field, wave frequency, and parallel component of the wave vector, respectively. The first and second terms in the brackets on the right hand side correspond to damping by electrons and protons, respectively. For weakly magnetized plasmas with $v_A < v_S$, proton damping always dominates the TTD for $\omega^2/k_{\parallel}^2 \sim v_S^2 \sim k_B T_p/m_p$.¹ If v_A does not change dramatically in the downstream, the continuous heating of background particles through the TTD processes makes $T_p \rightarrow (m_p/m_e)T_e$ since the heating rates are proportional to $(mT)^{1/2}$, where m and T represent the mass and temperature of the particles, respectively. We see that parallel propagating waves (with $\sin \theta = 0$) are not subject to the TTD processes and can accelerate some particles to relativistic energies through resonant interactions. Obliquely propagating waves are damped efficiently by the background particles. Although the damping rates for waves propagating

¹ For $T_e = T_p$, the electron damping term dominates when $v_A \geq 1.9 v_S$.

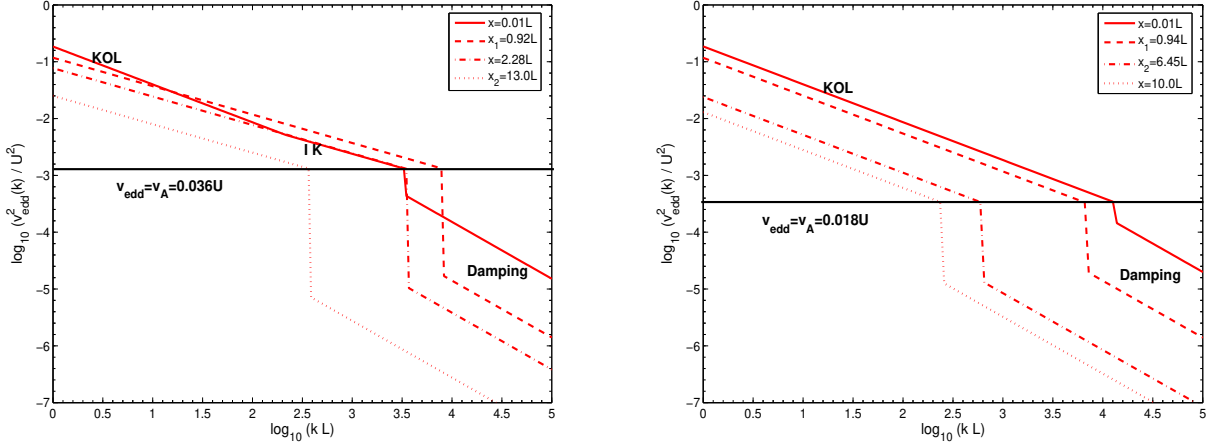


Figure 2. The angular-integrated compressional mode turbulence spectra $v_{edd}^2(k)$ at several locations in the downstream indicated in the legend for the speed profiles in Figure 1. In the dissipation range, it corresponds to $k\mathcal{W}$ instead of v_{edd}^2 . The onset of the TTD at k_d causes the discontinuity for the former. The left panel is for the Kraichnan phenomenology. The Kolmogorov, Kraichnan, and damping ranges are indicated for the supersonic phase spectrum with $x = 0.010L$. At the other locations, the turbulence is subsonic and there are only Kraichnan and damping ranges. The right panel is for the Kolmogorov phenomenology.

nearly perpendicular to the magnetic field ($\cos\theta \simeq 0$) are also low, these waves are subject to damping by magnetic field wandering (Petrosian et al. 2006).

The turbulence power spectrum cuts off sharply when the damping rate becomes comparable to the turbulence cascade rate (Jiang et al. 2009)

$$\Gamma = \tau_{edd}^{-1} \begin{cases} \tau_{edd}^{-1}/(\tau_F^{-1} + \tau_{edd}^{-1}) \simeq \tau_{edd}^{-1}\tau_F & \text{for IK,} \\ 1 & \text{for Kol.} \end{cases} \quad (35)$$

One can define a critical propagation angle $\theta_c(k)$, where $\Lambda_T(\theta_c, k) = \Gamma(k)$. Equations (31) and (34) then give

$$\frac{\sin^2\theta_c}{\cos\theta_c} \exp\left(-\frac{v_F^2}{2v_S^2 \cos^2\theta_c}\right) \simeq \begin{cases} v_A^2 k_d^{1/2}/(2^{-1/2}\pi^{1/2}v_S v_F k^{1/2}) & \text{for IK,} \\ v_A k_d^{1/3}/(2^{-1/2}\pi^{1/2}v_S k^{1/3}) & \text{for Kol.} \end{cases} \quad (36)$$

where the electron damping term has been ignored. The angular-integrated turbulence spectrum in the dissipation range is therefore given by

$$\begin{aligned} \mathcal{W}(k) &\simeq \frac{\theta_c^2(k)}{2} \begin{cases} u^{3/2} \min(v_F^{1/2}, u^{1/2}) k_m^{1/2} k^{-3/2} & \text{for IK,} \\ u^2 k_m^{2/3} k^{-5/3} & \text{for Kol.} \end{cases} \\ &\simeq \frac{\exp(5/6)v_A^3 k_d}{2^{1/2}\pi^{1/2}v_S} k^{-2} \begin{cases} v_A/v_F & \text{for IK,} \\ 1 & \text{for Kol.} \end{cases} \end{aligned} \quad (37)$$

Interestingly the turbulence spectrum is inversely proportional to k^2 in both scenarios. The angular-integrated turbulence spectra $\int W(k)2\pi k^2 d\cos\theta$ for the velocity profiles in Figure 1 at several locations in the downstream are shown in Figure 2. The discontinuities of the angular-integrated turbulence spectra are caused by the abrupt onset of thermal damping at the characteristic length l_d of the magnetic field. Obliquely propagating fast-mode waves are absorbed by the thermal background ions at this scale.

4 STOCHASTIC ELECTRON ACCELERATION BY FAST-MODE WAVES IN THE DOWNSTREAM

In a magnetized plasma, fast-mode waves are likely the agent responsible for efficient SA of electrons (Bykov & Toptygin 1983, 1993; Chandran 2003). The resonant interactions of particles with fast-mode waves have been studied by several authors (Miller, LaRosa & Moore 1996; Schlickeiser & Miller 1998; Petrosian & Liu 2004). In these studies, the authors prescribed the wave spectrum with several parameters and calculated the corresponding Fokker-Planck coefficients. A self-consistent treatment of the turbulence spectral evolution in the dissipation range was presented by Yan & Lazarian (2004) for a variety of astrophysical plasmas. Liu et al. (2006) considered the damping of fast-mode waves in a low- β plasma and the application of the SA of relativistic protons in magnetic field dominated funnels derived from general relativistic MHD simulations of non-radiative accretion flow around black holes. Section 3 shows that only fast-mode waves propagating parallel

to the local magnetic field can survive the TTD by the thermal ions in the high- β downstream plasma. These waves are right-handed polarized and resonate preferentially with electrons in the thermal background and therefore may selectively accelerate electrons to relativistic energies (Petrosian & Liu 2004). We next explore the SA of electrons in the shock downstream in this scenario.

We assume that the turbulence is isotropic from the turbulence generation scale L down to the dissipation scale $l_d = 1/k_d$, which depends on the turbulence speed u (Eq. [33]). Fast-mode waves are excited at the scale $l_F = 1/\max(k_t, k_m) = L/\max(1, u^3/v_F^3)$ and are also isotropic down to the dissipation scale. Due to the TTD, the energy density of fast-mode waves in the dissipation range is less than the magnetic field energy density. The resonant scatter rate of energetic particles by MHD waves is therefore smaller than v/l_d . However, for this high- β plasma, particles with a gyro-radius r_g less than the characteristic length of the magnetic field l_d drift along magnetic field lines with a scatter mean-free-path $l = v\tau_{sc} \leq l_d$. The scatter mean-free-path of particles with $r_g \simeq l_d$ should be comparable to $r_d \simeq l_d$ since particles with even higher energies scatter with the magnetic field randomly instead of performing gyro-motions. This efficient scatter of low-energy particles by the turbulence magnetic field results from bending of magnetic field lines by strong turbulence in the inertial range beyond l_d . The resonant wave-particle interactions in the dissipation range give a much lower scatter rate due to the strong damping of obliquely propagating fast-mode waves by thermal ions. Although this scatter through the particle gyro-motion and chaotic magnetic field structure is not caused by resonances with fast-mode waves, it determines the spatial diffusion coefficient $v^2\tau_{sc}/3 \simeq vl_d/3$, which plays essential roles in the SA by large-scale fast-mode waves (Ptuskin 1988).

The SA in the supersonic phase with $u > v_F$ is not well understood (Achterberg 1990; Bykov & Toptygin 1993). If we assume the turbulence speed u as the characteristic speed of the scatter agents and a scatter rate of l_d/c for relativistic particles with $r_g < l_d$, where c is the speed of relativistic particles, the acceleration rate will be comparable to that of the DSA. We also note that the turbulence speed u is higher than v_F in a narrow region near the SF (Fig. 1) corresponding to the turbulence generation. Such an SA will be difficult to distinguish from the first-order DSA. Further downstream, the turbulence speed is lower than v_F . We will ignore the particle acceleration in the supersonic phase and only consider the acceleration by acoustic waves in the subsonic phase, where Equation (16) is approximately applicable (Ptuskin 1988).

We assume $\tau_{sc} = l_d/v = l_d/c$ in the following for relativistic particles with $r_g \leq l_d$. Particles with even higher energies have a scatter time $\tau_{sc} \geq r_g/c$. The corresponding spatial diffusion coefficient is given by $D = \tau_{sc}c^2/3$ (Lagage & Cesarsky 1983). Following Ptuskin (1988), we have the acceleration timescale of these particles by a spectrum of fast-mode waves given by

$$\tau_{ac} = \left[\frac{8\pi D}{9} \int_{k_m}^{k_d} dk \frac{k^4 W(k)}{v_F^2 + D^2 k^2} \right]^{-1}. \quad (38)$$

The fast-mode turbulence also enhances the spatial diffusion of these particles. The incompressional modes are more efficient in enhancing the spatial diffusion than compressional modes (Bykov & Toptygin 1993). To include these effects and partially take into the effects of energy loss due to adiabatic expansion (Bykov & Toptygin 1983; Cowsik & Sarkar 1984), we adopt an effective diffusion coefficient:

$$D_* = D + \chi u L, \quad (39)$$

where χ is a dimensionless parameter. The escape time of relativistic electrons from the acceleration region is then given by

$$\tau_{esc} = (k_m^2 D_*)^{-1} = L^2/D_*. \quad (40)$$

Physically, χ needs to be less than 1, which corresponds to maximum diffusion caused by turbulence. However, considering the possible presence of incompressional modes and energy loss due to adiabatic expansion, the acceleration timescale by compressional modes will increase since the incompressional modes will carry part of the turbulence energy. The effect of this increase of acceleration timescale on the electron distribution can be partially taken into account by reducing the escape timescale, i.e., by increasing the effective spatial diffusion coefficient D_* . In what follows, we will treat χ as a free parameter with $\chi > 1$ indicating the presence of incompressional modes and reduction of acceleration by fast-mode waves. The presence of incompressional modes will also bring the transonic point closer to the SF. The acceleration by compressible modes in the subsonic phase can still be efficient. The details of these processes will depend on the coupling between compressible and incompressible modes (Petrosian & Bykov 2008) and is beyond the scope of this paper.

The dependence of acceleration and escape timescales on D at the transonic point in the downstream for typical conditions of SNR J1713.7-3946 are shown in Figure 3. The approximate acceleration timescale given by Equation (16) and the escape timescale due to the diffusion coefficient D alone, $(k_m^2 D)^{-1}$, are indicated with the thin lines. At high values of D , the slightly high discrepancy in the exact and approximate acceleration timescales of the Kraichnan phenomenology is due to the fact that the overall wave intensity is given by $2u^2$, instead of $3u^2/2$ as is for the Kolmogorov phenomenology.

When $Dk_m \gg v_F$, corresponding to the fast diffusion limit, $\tau_{ac} \simeq 3D/u^2$ and $\tau_{esc} \simeq (k_m^2 D)^{-1}$. Then $\tau_{ac}/\tau_{esc} \simeq 3D^2 k_m^2 / u^2 \gg 1$. The acceleration is negligible. With these asymptotic expressions for these timescales, the ratio of the acceleration to escape timescales decreases with the decrease of D and becomes close to unity near $D \sim u/(3^{1/2} k_m)$. Since

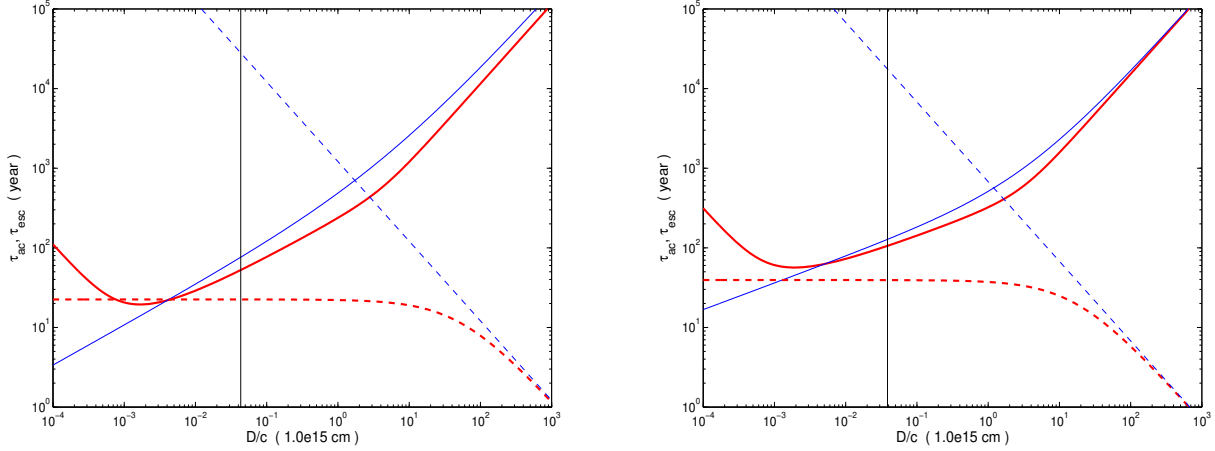


Figure 3. The acceleration (solid) and escape (dashed) timescales as a function of the diffusion coefficient D for conditions at the transonic point x_1 in the downstream, where $v_F = u$, for the Kraichnan (left with $\chi = 11$, $L = 10.7 \times 10^{17}$ cm and $v_A = 0.036U$) and Kolmogorov (right with $\chi = 4.7$, $L = 8.0 \times 10^{17}$ cm and $v_A = 0.018U$) phenomenology in Figure 1. $U = 4000$ km/s for both cases. The vertical line indicates the diffusion coefficient $D = cl_d/3$. The thick lines are the exact results given by Equations (38) and (40). The thin solid line indicates the approximate acceleration timescale given by Equation (16). The thin dashed line indicates $(k_m^2 D)^{-1}$. For a magnetic field of $B = 14\mu\text{G}$, the diffusion coefficient for TeV electrons is about $10^{15} c$ cm. The corresponding diffusion timescale over a length of $\sim 3 \times 10^{16}$ cm, the half-width of the variable X-ray filaments observed with *Chandra* (Uchiyama et al. 2007), is about one year.

deviations from these asymptotic expressions occur near $D \sim v_F/k_m \geq u/k_m$, efficient particle acceleration is only possible in the regime where $D < v_F/k_m$. When $Dk_d \ll v_F$, corresponding to the slow diffusion limit, $\tau_{ac} \simeq 3(5 - \delta)v_F^2/[(\delta - 3)Dk_d^{5-\delta}k_m^{\delta-3}u^2]$.

$$\tau_{ac} = \left[\frac{(\delta - 3)u^2}{3D} \left(\frac{Dk_m}{v_F} \right)^{\delta-3} \int_{k_m D/v_F}^{k_d D/v_F} dx \frac{x^{4-\delta}}{1+x^2} \right]^{-1} \simeq \left[\frac{(\delta - 3)u^2}{3D} \left(\frac{Dk_m}{v_F} \right)^{\delta-3} \int_0^\infty dx \frac{x^{4-\delta}}{1+x^2} \right]^{-1} \sim u^{-2} D (Dk_m/v_F)^{3-\delta}, \quad (41)$$

where $3 < \delta < 5$, which ensures the convergence of the integration. These results are in agreement with Figure 3.

The acceleration and escape timescales are determined by D and the turbulence spectrum. Since we assume that $D = l_d c/3$ for electrons with $r_g < l_d$, the electron acceleration and escape timescales are independent of the energy for $r_g < l_d$. When the ratio of acceleration to escape timescale is independent of the particle energy, a power-law particle distribution is expected in the steady-state with the spectral index given by (Ptuskin 1988)

$$p = \left(\frac{9}{4} + \frac{\tau_{ac}}{\tau_{esc}} \right)^{1/2} - \frac{1}{2}. \quad (42)$$

Since electrons with an energy less the proton rest energy can be scattered by whistler waves at small scales, the diffusion coefficient D for these particles can be much less than $l_d c/3$ and the corresponding spectral index $p \simeq 1$ (Petrosian & Liu 2004; Liu et al. 2006). The scatter will be dominated by the turbulent magnetic field before electrons reach the proton rest mass energy, the spectral break may appear below the proton rest mass energy. Without detailed treatment of these processes, we will assume that the electron distribution follows a power law with $p = 1$ for $\gamma \leq 10$ in the following.² Above $\gamma = 10$, the steady-state spectral index of the electron distribution is given by Equation (42) since the diffusion coefficient $D = l_d c/3$ is assumed to be independent of the electron energy. For relativistic electrons with $r_g \geq l_d$, $D \geq r_g c/3$. The increase of D with the electron energy E will lead to softening of the electron distribution toward higher energy dictated by the energy dependence of τ_{ac}/τ_{esc} . The exact electron distribution can be obtained numerically. For the sake of simplicity, we assume that the electron distribution has a high-energy cutoff at Lorentz factor

$$\gamma_c = \frac{qB}{m_e c^2 k_d} = \frac{qBLv_A^3}{m_e c^2 u^3} \begin{cases} v_A/\min(v_F, u) & \text{for IK,} \\ 1 & \text{for Kol.} \end{cases} \quad (43)$$

where q is the elementary charge units. Then for a steady-state treatment, the distribution of electrons escaping from the acceleration site may be approximated reasonably well with (Becker, Le & Dermer 2006; Park & Petrosian 1995)

² Assuming a spectral break at $\gamma = m_p/m_e$ will lead to a spectral bump near this break energy, in conflict with radio observations. This suggests that, when the acceleration time is long and p is high, one needs better treatment of the electron acceleration at low energies.

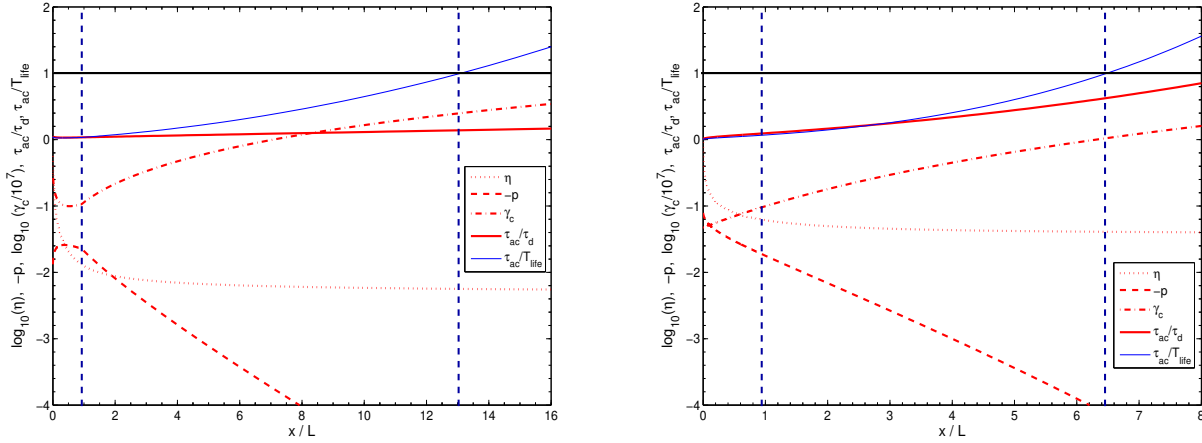


Figure 4. Evolution of the acceleration efficiency η (dotted), cutoff Lorentz factor γ_c (dotted-dashed), spectral index p (dashed), and $\tau = \tau_{ac}/T_{life}$ (thin solid) in the downstream for the Kraichnan phenomenology with $v_A = 0.036U$ and $\chi = 11$ (left) and Kolmogorov phenomenology with $v_A = 0.018U$ and $\chi = 4.7$ (right). $U = 4000$ km/s. The particle acceleration is significant for $\tau < 1$. We only consider acceleration between the two vertical dashed lines indicating x_1 and x_2 . For γ_c , we have assumed that $B = 14\mu\text{G}$, $L = 10.7 \times 10^{17}$ cm (left) and $B = 14\mu\text{G}$, $L = 8.0 \times 10^{17}$ cm (right).

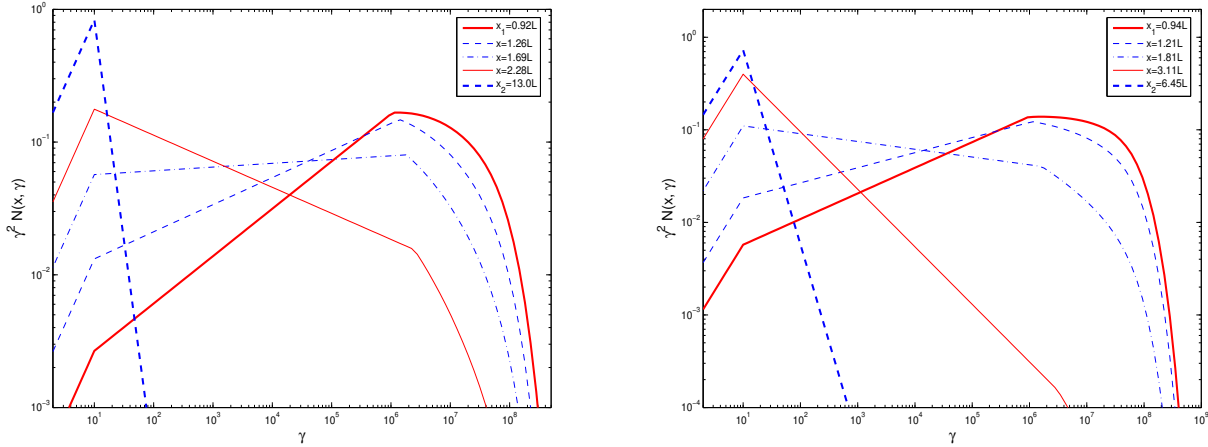


Figure 5. Normalized steady-state nonthermal electron distribution $f(x)$ produced at several locations in the downstream for the Kraichnan (left) and Kolmogorov (right) phenomenology in Figure 4.

$$f(x, \gamma) \propto \gamma^{-p(x)} \exp\{-[\tau_{ac}(D)/\tau_{esc}(D)]^{1/2}\}/\tau_{esc}(D), \quad (44)$$

where

$$D(\gamma, x) = \begin{cases} cl_d(x)/3 & \text{for } \gamma \leq \gamma_c(x), \\ cr_g(\gamma)/3 = \gamma m_e c^3 / (3qB) & \text{for } \gamma > \gamma_c(x). \end{cases} \quad (45)$$

We note that the shape of the distribution function near γ_c can also be affected by the energy loss processes (Stawarz & Petrosian 2008; Vannoni et al. 2009; Blasi 2010). In our model, it is mostly determined by the balance between the acceleration and escape processes (Park & Petrosian 1995; Becker, Le & Dermer 2006; Zirakashvili & Aharonian 2007). The shape of this high-energy cutoff has significantly effect on the fitting parameter, especially the value of γ_c . We are carrying out detailed numerical investigation of the particle distribution and the results will be reported in a separate publication.

Although the parallel propagating waves in the dissipation range may not contribute to the particle scatter significantly, energies carried by these waves are only accessible to relativistic electrons. At very small scales, these waves resonate with thermal background electrons giving rise to a preferential acceleration of electrons. One therefore may assume that the ratio of the dissipated energy carried by non-thermal electrons to that of the thermal ions is proportional to the ratio of the energy density of parallel propagating fast-mode waves to that of the magnetic field:

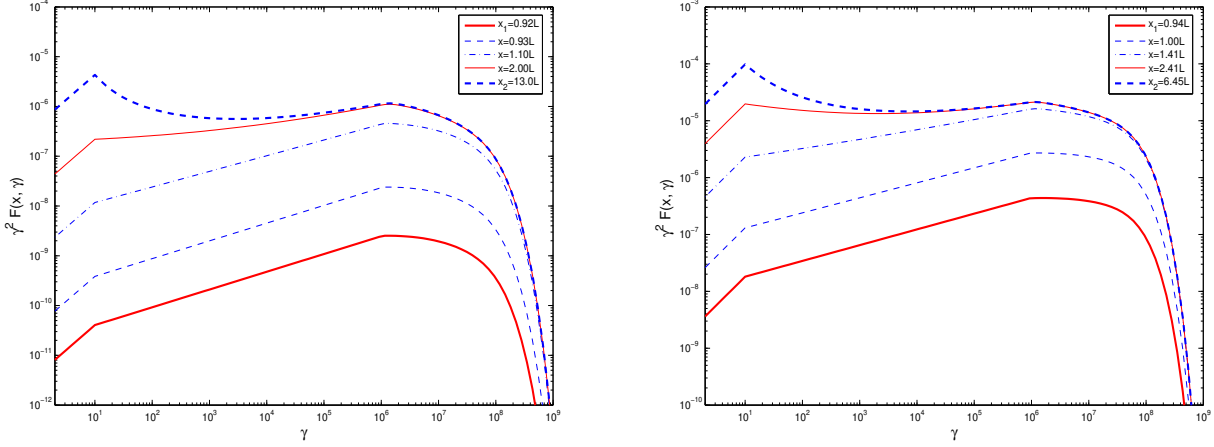


Figure 6. Distributions of nonthermal electrons $F(x)$ at several locations in the downstream for the Kraichnan (left) and Kolmogorov (right) phenomenology in Figure 4.

$$\eta = \frac{\theta_c^2(k_d)}{2} = \begin{cases} e^{5/6} v_A^2 / (2\pi)^{1/2} v_S v_F & \text{for IK,} \\ e^{5/6} v_A / (2\pi)^{1/2} v_S & \text{for Kol.} \end{cases} \quad (46)$$

where $e \simeq 2.72$ is the base of the natural logarithm. A more quantitative treatment of this issue may address the electron injection processes self-consistently (Eichler 1979b).

To have efficient acceleration of relativistic electrons, the turbulence decay time

$$\tau_d = 3L/C_1 u \begin{cases} \max(u, v_F)/u & \text{for IK,} \\ 1 & \text{for Kol.} \end{cases} \quad (47)$$

and the remnant lifetime T_{life} should be longer than the acceleration time. As we will see below, the turbulence decay time is always longer than T_{life} in the subsonic phase for SNR RX J1713.7-3946. There are at most two locations x_0 and x_2 with $x_0 < x_2$ in the downstream, where $\tau = \tau_{\text{ac}}/T_{\text{life}} = 1$. Figure 4 shows the evolution of η , γ_c , p , τ_{ac}/τ_d and $\tau = \tau_{\text{ac}}/T_{\text{life}}$ in the downstream for $U = 4000$ km/s. The profiles of v_F/U and u/U only depend on v_A/U . So is the profile of η . The profiles of τ and p also depend on the absolute value of U . To obtain γ_c , one needs to know L and B as well. Most SA occurs near the sonic point x_1 , where $v_F = u$. In the late subsonic phase, $u \ll v_F$, the SA is insignificant since most of the free energy of the system has been converted into heat. The characteristic length of the magnetic field is also long far downstream due to the weak turbulence, which implies long electron scatter and acceleration timescales.

Then the distribution of non-thermal electrons in the downstream

$$F(x, \gamma) = \int_{x_1}^x f(x', \gamma) \eta(x') (4Q/m_e c^2 U) dx' \quad (48)$$

where $\int_1^\infty \gamma f(x', \gamma) d\gamma = 1$, and $\int_1^\infty \gamma m_e c^2 F(x, \gamma) d\gamma$ gives the energy density of non-thermal particles at x . Figures 5 and 6 show the normalized electron distribution f and F for parameters in Figure 4 at several locations in the downstream, respectively. We note that the electron distribution has a rather gradual high-energy cutoff due to the weak dependence of the acceleration and escape timescales on the spatial diffusion coefficient D , which is proportional to the electron energy above the cutoff energy $\gamma_c m_e c^2$. This gradual cutoff results in a broad emission component due to inverse Comptonization of the low-energy background photons by high-energy electrons, which can fit the observed broad TeV emission spectrum from a few SNRs.

5 APPLICATION TO SNR RX J1713.7-3946 AND TIME-DEPENDENT MODELS

Here we use the SNR RX J1713.7-3946 as an example to demonstrate how the SA by fast-mode waves accounts for the observed broadband spectrum. The electron distribution produced by the SA is given by equation (48), where the integration over x' should stop at x_2 . Given the evolution history of the SNR, the nonthermal electron distribution will vary along the radial direction. A detailed modeling of the explosion is necessary to take this effect into account properly (Cowsik & Sarkar 1984; Zirakashvili & Aharonian 2010). Here we treat the volume of the emission region V_e as a free parameter to control the normalization of the emission spectrum, which is appropriate for SNRs where the nonthermal particles appear to be concentrated near the SF. By adjusting U , B , v_A , χ , L , and V_e , one can use the corresponding electron distribution $F(x_2)$

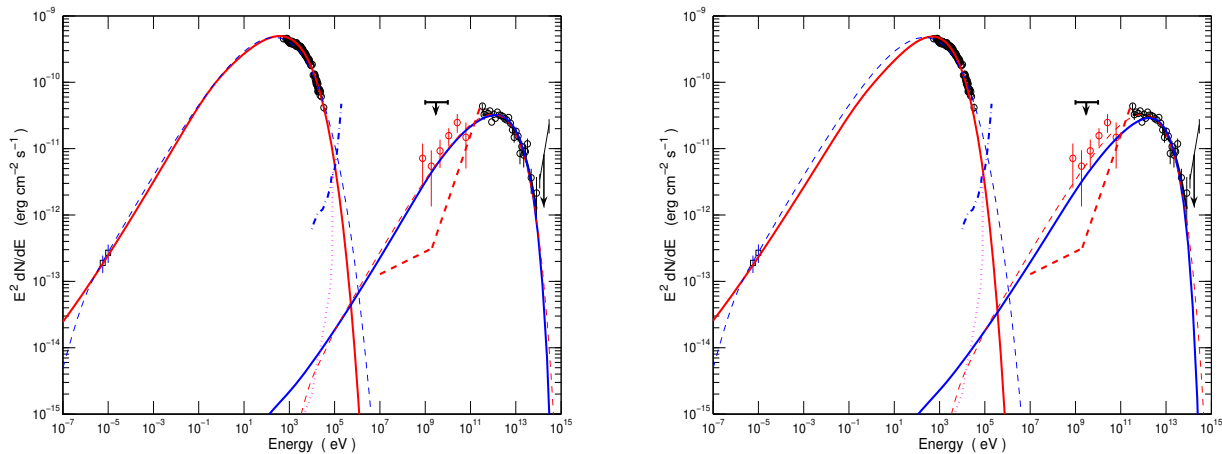


Figure 7. Best fits to the observed spectrum of the SNR RX J1713.7-3946. The X-ray data points are obtained from Tanaka et al. (2008). The other data points and the sensitivity limits of different high-energy telescopes are the same as those in Liu et al. (2008a). The left and right panels are for the Kraichnan and Kolmogorov phenomenology in Figure 4, respectively. The dashed line is for a simple power-law model with a gradual high-energy cutoff $F(\gamma) \propto \gamma^{1.85} \exp(\gamma/\gamma_c)^{1/2}$, where $\gamma_c m_e c^2 = 3.68$ TeV. The solid lines are for the fiducial models. The low and high energy spectral peaks are produced through the synchrotron and inverse Compton scatter of the background photons (Porter et al. 2006), respectively. The preliminary data from Fermi were not considered in the fit and are included here to show the agreement between model predictions and this observation (Funk 2009). The Fermi observation seems to favor the Kraichnan model.

Table 1. Model Parameters

model	U (km s ⁻¹)	B (μ G)	v_A/U	χ	L 10^{17} (cm)	V_e/V	E_e 10^{47} (erg)	ρ 10^{-26} (g cm ⁻³)
IK steady	4000	14.0	0.036	11	10.7	0.42	7.69	7.52
KOL steady	4000	14.0	0.018	4.7	8.0	0.016	6.96	30.1

to fit the observed spectrum of the SNR RX J1713.7-3946. Figure 7 shows the best fit with the corresponding parameters listed in Table 1, where V is the enclosed volume of the SNR SF. Comparing to the thin-dashed line, which is derived by assuming an electron distribution $\propto \gamma^{-p} \exp(-\gamma/\gamma_c)^{1/2}$, the high-energy cutoff of the Kraichnan model is more gradual than the Kolmogorov model, which makes the former spectrum broader. The emission volume is 0.42 (0.016) times the volume of the SNR for the Kraichnan (Kolmogorov) phenomenology, which is compatible with observations. The values of χ are greater than 1, which suggests that the particle spatial diffusion coefficient might be enhanced significantly by incompressible turbulence motions. The total energies of nonthermal electrons are also comparable to the magnetic field energy for a uniform magnetic field within the remnant, suggesting near energy equipartition between the nonthermal electrons and the magnetic field.

There are six parameters in the model: B , U , v_A , χ , L , and V_e . The observed radio to X-ray spectral index, X-ray to TeV flux ratio, location of the X-ray cutoff, and bolometric luminosity of the source give four constraints, which leads to two more degree of freedom. Our model fit to the spectrum therefore is not unique. χ is determined by the coupling between incompressible and compressible turbulence motions. B is well constrained by the ratio of the X-ray to TeV flux. To reproduce the observed spectral shape, the profiles of p , γ_c , and η should not change significantly, which implies that $v_A^8 c^2 \propto u^{10}$ and $L \propto u^4/v_A^4$ at the transonic point for the Kraichnan phenomenology. For the Kolmogorov model, $v_A^8 c^2 \propto u^8$ and $L \propto u^3/v_A^3$. For $v_A \ll U$, u is proportional to U , we find that nearly identical emission spectra can be obtained by adjusting U and v_A (Liu et al. 2008b). Since the turbulence decay time is longer than the supernova lifetime, the steady-state treatment is also justified. A time-dependent treatment gives identical parameters (Becker, Le & Dermer 2006).

6 DENSITY AND TURBULENCE GENERATION

The primary discrepancy between these models and the observations are the relatively high densities of the downstream plasma. From X-ray observations, Cassam-Chenaï et al. (2004) inferred an upper limit for the electron density of 0.02 cm⁻³. The corresponding mass density is about 3.3×10^{-26} g cm⁻³, which is comparable to the densities inferred with the Kraichnan phenomenology but lower than those inferred with the Kolmogorov phenomenology. On the other hand, the electron tempera-

ture could be much lower than the ion temperature in the shock downstream (Zirakashvili & Aharonian 2010). Morlino et al. (2009) and Fang et al. (2009) have argued that the density in the downstream can be as high as 0.5 cm^{-3} , corresponding to a mass density of $8.4 \times 10^{-25} \text{ g cm}^{-3}$.

Given the age of $T_{\text{life}} = 1600$ years and a radius of $R = 10$ pc at a distance of $D \simeq 1$ kpc, the corresponding average speed of the shock front is 6100 km s^{-1} . With the self-similar solution of Chevalier (1982), we infer a shock speed of $[(n-3)/(n-s)]6100 \text{ km s}^{-1}$, where $n > 5$ and $0 \leq s < 3$ are the power-law exponents of the density profile for the ejecta and the ambient medium, respectively. Observations give an upper limit of 4500 km s^{-1} for the shock speed (Uchiyama et al. 2007). From the self-similar solution, the shock speed must be higher than 2400 km s^{-1} (for $s = 0$ and $n = 5$). If ions are preferentially heated by the shock, the corresponding ion temperature T_i will be higher than $3m_p U^2/16k_B > 1.3 \times 10^8 \text{ K}$. The electron temperature should be higher than that given through Coulomb collisional energy exchange with ions (Hughes et al. 2000):

$$T_e > 2.1 \times 10^7 (T_{\text{life}}/1600 \text{ yr})^{2/5} (n_e/\text{cm}^{-3})^{2/5} (T_i/1.3 \times 10^8 \text{ K})^{2/5} \text{ K}, \quad (49)$$

where n_e is the electron number density. The corresponding bremsstrahlung luminosity is $\mathcal{L} > 5.2 \times 10^{34} (n_e/0.5 \text{ cm}^{-3})^{11/5} \text{ erg s}^{-1}$, which is comparable to the luminosity of the observed nonthermal X-ray emission.³ We therefore expect strong thermal emission with such a high density. Morlino et al. (2009) obtained a very low thermal bremsstrahlung luminosity by arbitrarily adopting an electron temperature 100 times lower than the ion temperature. As shown above, considering the electron ion Coulomb collisional energy exchange, the electron temperature will not be that low and significant thermal X-ray is expected with a density of 0.5 cm^{-3} , except that cooling of the shock front by cosmic ray ions dominates (Zirakashvili & Aharonian 2010). The highest electron density given by our models is about 0.2 cm^{-3} . The corresponding thermal X-ray luminosity will be reduced by nearly one order of magnitude and should be in agreement with observations. Detailed modeling of the supernova explosion and the thermal emission is needed to see the validity of these models.

The model inferred density may also be reduced by considering the acceleration of electrons by large-scale structures in the downstream and the acceleration in the supersonic phase, where the first-order Fermi acceleration is also possible. In this paper, we consider the electron acceleration by the fully developed turbulence in the subsonic phase. It assumes that once the electrons diffuse over a scale of the turbulence generation length L , the acceleration stops. As shown above, the turbulence evolves in the downstream. In a more self-consistent treatment, one may use the turbulence properties to derive nonthermal electrons injected into the downstream flow by small scale plasma waves and consider the further acceleration of these electrons as they diffuse spatially in the downstream. The scatter mean-free-path of these particles are determined by the properties of turbulence. The electron acceleration stops only after they diffuse into upstream or far downstream, where the turbulence becomes insignificant. If these effects lead to a harder overall electron distribution, the Alfvén speed needs to be increased to fit the observations, leading to a lower density.

From these models studied here, we see that, to have efficient SA, both high-speed waves ($v_F \simeq u$) and short scatter mean-free-path are required. Quantitatively, one needs $c^2 l^2/L^2 u^2$ to be on the order of unity so that the acceleration and escape time scales of relativistic particles are comparable. u is constrained by the shock speed. A short scatter mean-free-path is achieved by the reduction of the characteristic length of the magnetic field, which also determines the maximum energy of the accelerated particles. In these models, turbulence motions are invoked to reduce the characteristic length of the magnetic field. It is obvious, such a mechanism is only possible for strong turbulence, where the turbulence speed is higher than the Alfvén speed. The turbulence speed is determined by the shock speed $u \leq (3/16)^{1/2} U$, which is less than 1949 km s^{-1} for SNR RX J1713.7-394. Therefore $v_A < 1949 \text{ km s}^{-1}$ and we obtain a low limit for the mass density from the inferred magnetic field of $14 \mu\text{G}$: $\rho = B^2/4\pi v_A^2 > 4.1 \times 10^{-28} \text{ g cm}^{-3} (B/14\mu\text{G})^2 (U/4500 \text{ km s}^{-1})^{-2}$, which corresponds to an electron density of $\sim 0.0002 \text{ cm}^{-3} (B/14\mu\text{G})^2 (U/4500 \text{ km s}^{-1})^{-2}$.

Therefore further reduction of the density can be achieved by considering the generation of the turbulence and its effect on the turbulence spectrum, i.e., the dependence of the eddy velocity on the spatial scale. Indeed, in the models considered above, we assume that the turbulence is generated in a very narrow spatial range instantaneously at the SF and an inertial range develops. Since the large-scale eddy speed is comparable to the bulk velocity of the downstream flow moving away from the shock front, the region with $x < 0.5$ should be considered as the turbulence generation phase. This is an intrinsic limitation of the above treatments, which focus on the averaged properties of the downstream flow without addressing the turbulence generation process. Significant particle acceleration occurs within $x < 0.5$, i.e., the turbulence generation phase. It is also possible that the turbulence is generated over a broad spatial range and/or the turbulence is not isotropic at large scales. One then expects a turbulence spectrum shallower than the initial range spectrum. For example, for a turbulence spectrum of

$$W = [3u^2/8\pi(g-3)](2\pi/L)^{g-3} k^{-g-2} \quad (50)$$

³ Here we have assumed an emission volume one quarter of the volume enclosed by the remnant shock front.

with $1 < g < 1.5$,⁴ where the normalization is chosen so that the turbulence energy density is given by $(3/2)\rho u^2$, the eddy speed can be redefined as

$$v_{edd} \equiv \{[8\pi(g-1)/3]k^3W\}^{1/2} = u(kL/2\pi)^{(1-g)/2}. \quad (51)$$

The eddy speed is comparable to the Alfvén speed at the characteristic length of the magnet field l , we then have $12c^2l^2/v_f^2L^2 = 12c^2v_A^{4/(g-1)}/v_f^2u^{4/(g-1)} \sim 1$. Therefore $v_A/u \sim (v_f/12c)^{(g-1)/2}$. Since $v_f \sim u \sim U$, we have $v_A/U \sim (U/c)^{(g-1)/2}$. The Alfvén speed can be comparable to the turbulence speed for a shallow turbulence spectrum with g approaching 1. Thus stochastic electron acceleration can account for observations of SNR RX J1713.7-394 as far as the mass density of the shocked plasma is greater than $4.1 \times 10^{-28} \text{ g cm}^{-3}$. Detailed studies of the turbulence generation and the associated particle acceleration are warranted (Lucek & Bell 2000; Hededal et al. 2004; Giacalone & Jokipii 2007; Nishikawa et al. 2009).

7 SUMMARY AND CONCLUSIONS

In the paper, we study the SA of electrons by a decaying turbulence as produced and/or enhanced by strong non-relativistic shocks and carried away from the SF with the downstream flow. It is shown that, to have significant particle acceleration, the turbulence must cover a large spatial scale so that the particle acceleration time may be shorter than the turbulence decay time. To account for observations of a few STTSNRs with the leptonic scenario for the TeV emission, fast-mode waves need to be excited in the subsonic phase. Given the turbulent nature of the downstream flow, fast-mode waves may prevail in the downstream. We show that the SA by large-scale acoustic (fast-mode) waves can account for the observations.

There are four basic model parameters, namely, the magnetic field, mass density, shock speed, and the turbulence generation scale. Observations of a few SNRs and radio galaxies have shown that the particle acceleration may change dramatically along the SF (Rothenflug et al. 2004; Reynolds 2009; Croston et al. 2009). This variation has been attributed to a large-scale magnetic field in the DSA model as the acceleration efficiency varies with the angle between the magnetic field and the shock normal. With our model, this variation is likely caused by a quite different mechanism. Detailed comparative studies should be able to distinguish these models.

The particle acceleration is very sensitive to the magnetic field. To produce nonthermal particle distribution in compatible with observations, $c^2v_A^8/u^{10}$ and $c^2v_A^6/u^8$, where u is the large-scale eddy speed near the shock front, should be on the order of 1 for the Kraichnan and Kolmogorov phenomenology, respectively. The high-energy cutoff of the particle distribution is determined by the magnetic field and the turbulence generation scale. Weaker fields will lead to lower cutoff energies and harder spectra. The particle acceleration may be turned off completely for strong fields due to the increase of the characteristic length of the magnetic field, and therefore the particle scatter mean-free-path. If the magnetic field is predominantly generated by the streamline of nonthermal particles upstream, the models then imply $v_A \sim U^{5/4}$ and $v_A \sim U^{4/3}$ for this dynamo process and for the Kraichnan and Kolmogorov phenomenology in the downstream turbulence, respectively.

Assuming that the turbulence is isotropic and generated in a narrow spatial scale, the model inferred densities of the downstream flow may be so high that thermal X-ray emission becomes observable, in conflict with observations. Although the thermal X-ray emission may be suppressed by a lower electron temperature due to dominance of the cooling by cosmic ray ions, we find that a low density is also possible if the turbulence is not isotropic or generated over a broad spatial scale so that the eddy speed has very weak dependence on the spatial scales. Detailed modeling of the progenitor and the evolution history of the remnant may help to constrain the density (Cowsik & Sarkar 1984).

The application of the models to the SNR RX J1713.7-3946 also suggests energy equipartition between the magnetic field and the acceleration electrons. If the rest of the shock energy is dissipated as heat in the downstream, then the overall electron acceleration efficiency will be $\sim v_A^2/u^2$, which is inversely proportional to the plasma β of the downstream flow. For the Kraichnan phenomenology, $v_A^2/u^2 \sim (u/c)^{1/4}$ and for the Kolmogorov phenomenology $v_A^2/u^2 \sim (u/c)^{1/3}$, acceleration is more efficient for stronger shocks, which also produce hotter downstream plasma. However, the dependence of the acceleration efficiency on the shock speed is rather weak. These may have significant implications on the origin of cosmic rays and their connection to the properties of the interstellar medium (Reynolds 2008).

With the fast-mode wave turbulence model studied in this paper, relativistic electrons may also be accelerated through the first-order Fermi mechanism as in the DSA model, especially in the supersonic phase. The high-energy cutoff can still result from decoupling of higher energy particles with the background magnetic field as their gyro-radius exceeds the characteristic length of the magnetic field. This is quite different from the DSA models, where the high-energy cutoff is related to a finite lifetime of the shock, shock curvature, or efficient energy loss processes (Zirakashvili & Aharonian 2010).

⁴ For $g < 1$, the eddy speed increases with the decrease of the spatial scale and the turbulence energy is not dominated by the large scale eddies. One then needs to introduce a spectral break at certain small scale. Such a complex scenario is not well justified from both observational and theoretical point of views.

ACKNOWLEDGEMENTS

We thank the referee for critical reviews of the paper, which made us examine the acceleration timescale and the shape of the high-energy cutoff of the electron distributions carefully. SL acknowledges support from the EU's SOLAIRE Research and Training Network at the University of Glasgow (MTRN-CT-2006-035484) and thanks Lyndsay Fletcher for constant support and John Kirk and Christian Fendt for invitation to the workshop entitled "The high-energy astrophysics of outflows from compact object", where some ideas in this paper were conceived. This work is supported in part under the auspices of the US Department of Energy by its contract W-7405-ENG-36 to Los Alamos National Laboratory and by the National Science Foundation of China (grants 10963004 and 10778702), Yunnan Provincial Science Foundation of China (grant 2008CD061) and SRFDP of China (grant 20095301120006).

REFERENCES

- Aharonian, F. A., et al. 2006, *A&A*, 449, 223
 Aharonian, F. A., et al. 2007, *ApJ*, 661, 236
 Achterberg, A. 1979, *A&A*, 76, 276
 Achterberg, A. 1990, *A&A*, 231, 251
 Atoyan, A. M., Aharonian F. A., Tuffs, R. J., & Völk, H. J. 2000, *A&A*, 355, 211
 Ball, L., Melrose, D. B., & Norman, C. A. 1992, *ApJ*, 398, 65
 Bell, R. A. 1978, *MNRAS*, 187, 142
 Becker, P. A., Le, T., & Dermer, C. D. 2006, *ApJ*, 647, 539B
 Beresnyak, A., & Lazarian, A. 2008, *ApJ*, 678, 961
 Blandford, R., & Eichler, D. 1987, *Phys. Reports*, 154, 1
 Blasi, P. 2010, *MNRAS*, 402, 2807
 Butt, Y. M., Porter, T. A., Katz, V., & Waxman, E. 2008, *MNRAS*, 386, L20
 Butt, Y. M. 2009, *Nature*, 460, 701
 Bykov, A. M., & Toptygin, I. N. 1983, in *Int. Cosmic Ray Conf.*, Vol. 9, 313
 Bykov, A. M., & Toptygin, I. N. 1993, *Phys. Uspekhi*, 36, 1020
 Cassam-Chenaï, G., Decourchelle, A., Ballet, J., Sauvageot, J. L., Dubner, G., & Giacani, E. 2004, *A&A*, 427, 199
 Chandran, B. 2003, *ApJ*, 599, 1426
 Chevalier, R. A. 1982, *ApJ*, 258, 790
 Cho, J., & Lazarian, A. 2006, *ApJ*, 638, 811
 Cho, J., & Vishniac, E. T. 2000, *ApJ*, 538, 217
 Cowsik, R., & Sarkar, S. 1984, *MNRAS*, 207, 745
 Croston, J. H. et al. 2009, *MNRAS*, 395, 1999
 Dickel, J. R., van Breugel, W. J. M., & Strom, R. G. 1991, *AJ*, 101, 2151
 Eichler, D. 1979a, *ApJ*, 229, 409
 Eichler, D. 1979b, *ApJ*, 229, 413
 Eichler, D. 1979c, *ApJ*, 229, 419
 Eilek, J. A. 1979, *ApJ*, 230, 373
 Fang, J., Zhang, L., Zhang, J. F., Tang, Y. Y., & Yu, H. 2009, *MNRAS*, 392, 925
 Fermi, E. 1949, *Phys. Rev.*, 75, 1169
 Fisk, L. A., & Gloeckler, G. 2007, *Proc. Natl. Acad. Sci. USA*, 104, 5749
 Funk, S. 2009, *Fermi Symposium*, <http://fermi.gsfc.nasa.gov/science/symposium/2009/program.html>
 Giacalone, J., & Jokipii, J. R. 2007, *ApJ*, 663, L41
 Ginzburg, V.L., & Ptuskin, V. S. 1976, *Reviews of Modern Physics*, 48, 161
 Goldreich, P., & Sridhar, S. 1995, *ApJ*, 438, 763
 Hededal, C. B., Haugbolle, T., Frederiksen, J. T., & Nordlund, A. 2004, *ApJ*, 617, L107
 Hughes, J. P., Rakowski, C. E., & Decourchelle, A. 2000, *ApJ*, 543, L61
 Iroshnikov, P. S. 1963, *Astron. Zh.*, 40, 742
 Jiang, Y. W., Liu, S. M., & Petrosian, V. 2009, *ApJ*, 698, 163
 Kirk, J. G., & Duffy, P. 1999, *J. Phys. G: Nucl. Part. Phys.*, 25, R163
 Kolmogorov, A. 1941, *DoSSR*, 30, 301
 Kraichnan, R. 1965, *Phys. Fluids*, 8, 1385
 Lacombe, C. 1977, *A&A*, 54, 1
 Lagage, P. O., & Cesarsky, C. J. 1983, *A&A*, 125, 249
 Liu, S. M., Melia, F., Petrosian, V., & Fatuzzo, M. 2006, *ApJ*, 647, 1099

- Liu, S. M., Fan, Z. H., Fryer, C. L., Wang, J. M., & Li, H., 2008a, *ApJ*, 683, L163
- Liu, S. M., Fan, Z. H., & Fryer, C. L. 2008b, *Proceeding of the 4th International Meeting on High Energy Gamma-Ray Astronomy*. AIP conference Proceedings, 1085, 344
- Lucek, S. G., & Bell, A. R. 2000, *MNRAS*, 314, 65
- Micono, M., Zurlo, N., Massaglia, S., Ferrari, A., & Melrose, D. B. 1999, *A&A*, 349, 323
- Miller, J. A., LaRosa, T. N., & Moore, R. L. 1996, *ApJ*, 461, 445
- Morlino, G., Amato, E., & Blasi, P. 2009, *MNRAS*, 392, 240
- Niemiec, J., Pohl, M., Stroman, T., & Nishikawa, K. I. 2008, *ApJ*, 684, 1174
- Nishikawa, K. I., et al. 2009, *ApJ*, 698L, 10
- Park, B. T., & Petrosian, V. 1995, *ApJ*, 446, 699
- Petrosian, V., & Bykov, A. M., 2008, *SSRv*, 134, 207
- Petrosian, V., & Liu, S., 2004, *ApJ*, 610, 550
- Petrosian, V., Yan, H. R., & Lazarian, A. 2006, *ApJ*, 644, 603
- Pryadko, J. M., & Petrosian, V. 1997, *ApJ*, 482, 774
- Plaga, R. 2008, *NewA*, 13, 73
- Porter, T. A., Moskalenko, I. V., & Strong, A. W. 2006, *ApJ*, 648L, 29
- Ptuskin, V. S. 1988, *Soviet Astron. Lett.*, 14, 255
- Reynolds, S. P. 2008, *Annu. Rev. Astro. Astrophys.* 46, 89
- Reynolds, S., Borkowski, K., Green, D., Hwang, U., Harrus, I., Petre, R. 2009, *ApJ*, 695, L149
- Rothenflug, R., Ballet, J., Dubner, G., Giacani, E., Decourchelle, A., & Ferrando, P., 2004, *A&A*, 425, 121
- Schlickeiser, R., & Miller, J. A. 1998, *ApJ*, 492, 352
- Scott, J. S., & Chevalier, R. 1975, *ApJ*, 197, L3
- Stix, T. H. 1962, *The Theory of Plasma Waves* (McGraw-Hill Book Company, inc.)
- Stawarz, L., & Petrosian, V. 2008, *ApJ*, 681, 1725
- Tanaka, T., et al. 2008, *ApJ*, 685, 988
- Tidman, D. A., & Krail, N. A. 1971, *Shock Waves in Collisionless Plasmas* (Wiley-Interscience, John Wiley & Sons, Inc. New York, London, Sydney, Toronto)
- Treumann, R. A., & Jaroschek, C. H. 2008, *PRL*, 100, 155005
- Uchiyama, Y., Aharonian, F., Tanaka, T., Takahashi, T., Maeda Y. 2007, *Nat*, 449, 576
- Vannoni, G., Gabici, S., & Aharonian, F. A. 2009, *A&A*, 497, 17
- Wang, Z. R., Qu, Q.-Y., & Chen, Y. 1997, *A&A*, 318L, 59
- Yan, H., & Lazarian, A. 2004, *ApJ*, 614, 757
- Yeung, P. K., & Zhou, Y. 1997, *PhRvE*, 56, 1746
- Zhou, Y., & Matthaeus, W. H. 1990, *JGR*, 95, 14881
- Zirakashvili, V. N., & Aharonian, F. A. 2007, *A&A*, 465, 695
- Zirakashvili, V. N., & Aharonian, F. A. 2010, *ApJ*, 708, 965

This paper has been typeset from a \TeX / \LaTeX file prepared by the author.